A Comparison of Some Methods for Direct 2D Reconstruction from Discrete Projected Views

Preeti Gopal[1,2](✉), Ajit Rajwade[1], Sharat Chandran[1], and Imants Svalbe[3]

[1] Department of CSE, IIT Bombay, Mumbai, India
{preetig,ajitvr,sharat}@cse.iitb.ac.in
[2] IITB-Monash Research Academy, Mumbai, India
[3] School of Physics and Astronomy, Monash University, Clayton, Australia
imants.svalbe@monash.edu

Abstract. Tomographic acquisitions can be described mathematically as discrete projective transforms. Direct reconstruction methods aim to compute an accurate inverse for such transforms. We assemble a limited set of measurements and then apply the inversion to obtain a high-fidelity image of the original object. In this work, we compare the following direct inversion techniques for sets of discrete projections: Radon-i(inverse)Radon, a least squared error method and filtered back-projection for Mojette inversion. We observe that filtered back-projection is the best of these methods, as the reconstruction errors that arise using this method depend least strongly on the image structure. We aim to improve results for the filtered back-projection method by optimizing the design of the regularizing filter and here present work towards eliminating the regularization threshold that is used as part of this method.

1 Introduction

The classic Radon transform is based on the continuous spatial domain and requires infinitely many projections for exact reconstruction [1], which is practically infeasible. Thus, the inverse Radon transform is an ill-posed problem. This lead to the evolution of Discrete Radon Transform (DRT) in which the underlying object is viewed as a discrete entity rather than a continuous entity. Digital projections are computed along specific set of angles and if the number of angles is sufficient, then exact inversion is possible. However, in practice, the trajectory of X-rays does not follow discrete paths. The acquired measurements, which are in Radon form, can be converted to equivalent discrete measurements by solving a system of equations, as described in [2].

A type of DRT, called the Mojette transform, was developed by Guédon *et al.* [3]. The advantage of this transform is that, if a sufficiently large number of angles are used, then direct back-projection of discrete Mojette projections results in exact recovery of the image [4], and is reasonably robust to noise [5,6]. Each discrete projection angle is defined by a set of numbers: (p, q) where p and q are co-prime integers. Computing projection along (p, q) involves summing the intensity values of pixels that lie along the line making an angle of $\tan^{-1}\frac{p}{q}$.

This procedure is also termed as 'Dirac' Mojette transform because the underlying 2D pixel representation is a 'Dirac' field, i.e.

$$f(x, y) = \sum_k \sum_l f(k, l)\delta(x - k)\delta(y - l) \qquad (1)$$

Here, there is no notion of interpolation like the Radon transform as every pixel is considered to be a weighted Dirac function [7]. The Dirac Mojette transform is formally defined as:

$$M(b, p, q) = Projection_{pq}(b)$$
$$= \sum_{k=-\infty}^{+\infty} \sum_{l=-\infty}^{+\infty} f(k, l)\delta(b + kq - pl) \qquad (2)$$

where $\delta(n)$ is the kronecker delta function with value 1 when $n = 0$ and 0 everywhere else. Thus, values of all pixels that lie on the line $kq - pl = b$ are summed and put into the bin b. Both Mojette forward projection and inverse transforms of an image can be computed with the same complexity, given by $O(IN)$ [8]. Thus it is linear in I, the number of projections and N, total number of pixels in an image. The number of bins required for a projection is given by:

$$\text{Nbins(i)} = (W - 1) * |p_i| + (H - 1) * |q_i| + 1 \qquad (3)$$

It is thus dependent on the angle (p_i, q_i), and the image size $H \times W$. In order to uniquely reconstruct this image, the following criterion [9] must be satisfied by the chosen angle set:

$$W \leq \sum_i |p_i| \text{ or } H \leq \sum_i |q_i| \qquad (4)$$

This is called the Katz sufficiency criterion. Our aim is to perform image reconstructions below the Katz limit. When this sufficiency criterion is not met, the 'missing' projections give rise to reconstruction artefacts (called 'ghosts') [10].

Our aim here is to evaluate several methods to invert discrete projection data from a limited set of (p, q) view angles. This work is part of a study [11] reconstructing 3D and 4D image data under sparse assumptions by pooling projections across multiple 2D 'slices'. Direct reconstructions of 2D slices will be used as seeds for iterative reconstruction methods or as part of the guiding mechanism used to select and pool slices.

We seek optimal and robust 2D image reconstruction using minimal projection data. The goal of this paper is to compare three methods of direct tomographic reconstruction: classical Radon-i(inverse) Radon, filtered back-projection and a least squared error driven filtered back-projection method. We have not analyzed corner-based inversion [7], because it is noise intolerant; the Finite Radon Transform (FRT) [12], as it requires a fixed set of view angles and has strong image artefacts when the available data is under-sampled; and iterative multi-scale methods- as they work best for selected combinations of (p, q) view angles. We will include the recently published fractional Fourier method of Kingston [13] in our future work.

2   Direct Inversion Methods

We compared the performance of the following three reconstruction techniques on a set of images shown in Fig. 1:

1. Shepp-Logan inverse Radon (filtered back-projection) on Radon projected images.
2. Point Spread Function (PSF) estimation by least squared error method on Mojette projected images.
3. Filtered back-projection on Mojette projected images.

The circular mask of the images constrains the reconstructed views to have equal projection lengths for all view angles (as is common for CT where the ROI shape is framed by the edges of a rotating X-ray beam). A set of discrete angles was used for computing projections. Each angle consisted of (p, q) where p and q are co-prime integers. Throughout this paper, we refer to the 'shortest' angles as those which have small $\sqrt{p^2 + q^2}$ values. Thus, the first six shortest angles are $(0, 1)$, $(1, 0)$, $(1, 1)$, $(-1, 1)$, $(2, 1)$ and $(-2, 1)$. For all the experiments described in this section, the shortest 52 angles were used. To measure the quality of reconstructed images, we have used the Mean Squared Error (MSE) based Peak Signal to Noise Ratio (PSNR), as a metric.

2.1   Radon-iRadon

We computed the Radon projection along a fixed set of angles, each being given by $\tan^{-1}\frac{p}{q}$, corresponding to the discrete angle (p, q). Following this, the image was reconstructed using Shepp-Logan filtered back-projection for inverse Radon. The use of Shepp-Logan filter is a compromise between applying no filter (Ram-Lak) and the more heavy noise suppression of filters like Cosine or Hamming (We synthesize our projections by forward projection of the image data. Hence noise is not a major problem here). The results are shown in Fig. 2.

2.2   Least Squared Error Method

The Mojette back-projected image m and the original image im are related by the following expression [7]:

$$m_{p,q}(x, y) = im(x, y) * h_{p,q}(x, y) \qquad (5)$$

where $h_{p,q}$ denotes the PSF corresponding to the Mojette angle set (p, q) along which the projections are taken and $*$ denotes convolution operator. In the frequency domain, we have

$$M(u, v) = IM(u, v) \cdot H(u, v) \qquad (6)$$

We estimated $1/H(u, v)$ using a least squared error technique. The sum of $((1/H) \cdot M - IM)^2$ is minimized over all the training images. The resultant PSF
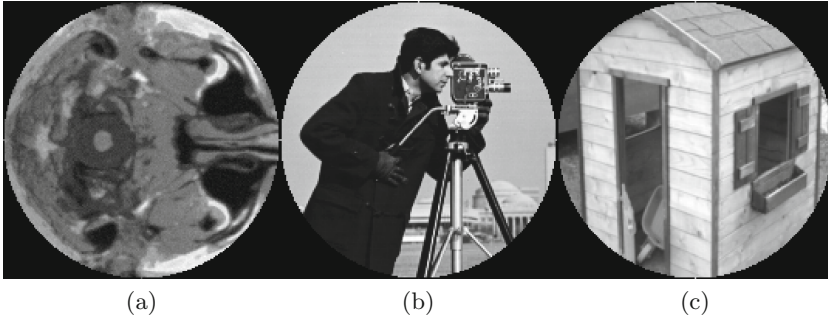
Fig. 1. Original images used for testing reconstruction algorithms throughout this paper. (a): Slice of the brain [14], (b): Cameraman, (c): House. Each image is of size 179×179

(a) PSNR = 21.24   (b) PSNR = 17.43   (c) PSNR = 19.66
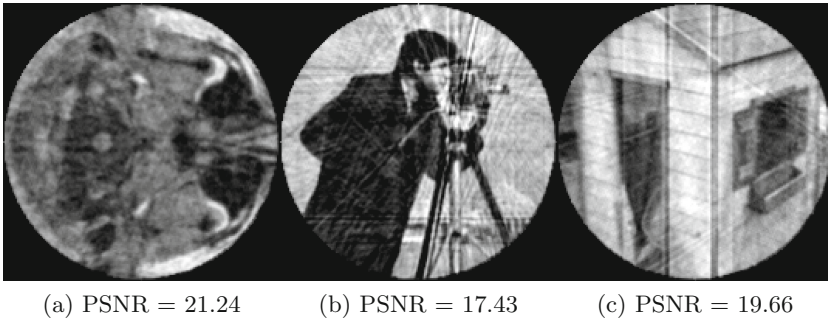
Fig. 2. Reconstruction by Radon-iRadon technique with the 52 shortest projection angles
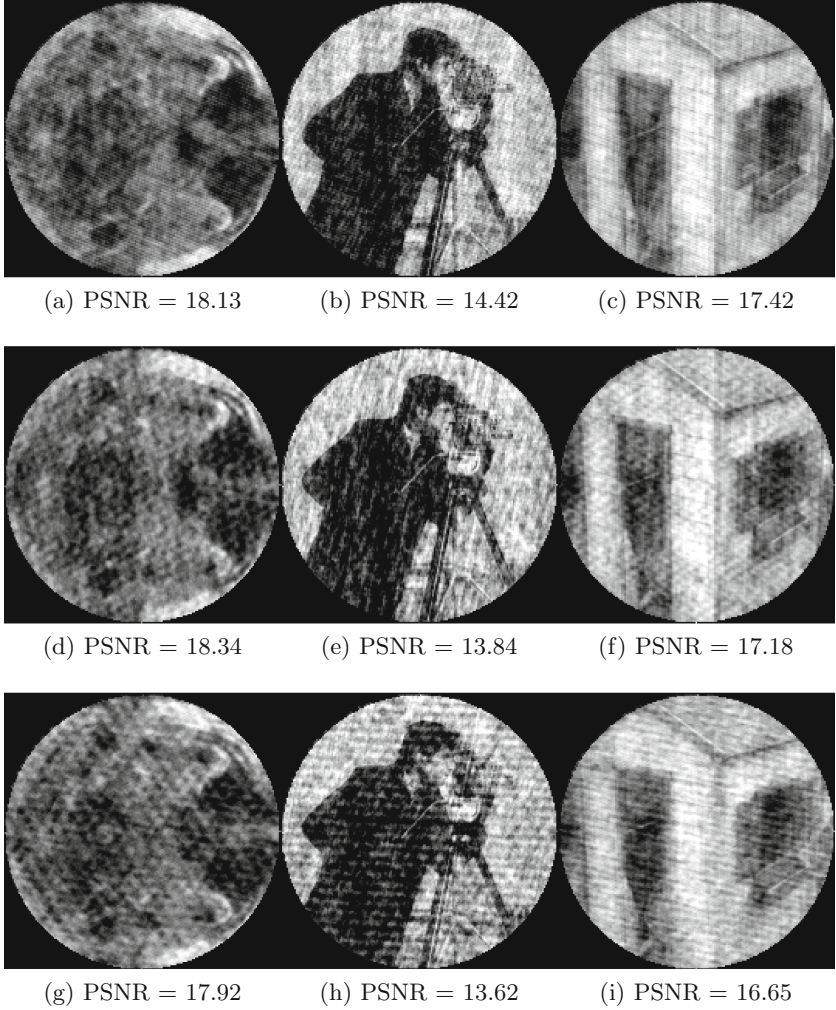
is checked for extremely small values (below a fixed threshold) and these values are replaced by the mean of their neighborhoods. The training set included 10 randomly chosen images from a dataset of images of birds and natural scenery. The size of the training set did not affect the quality of estimation. A small training set with 10 images was found to give results which were similar to those when 100 or 500 training images were used. This is because the PSF is not entirely image dependent. Its value (when estimated this way) is erroneous only in those locations where the 0/0 problem arises, because of which specific structural artefacts were observed in the reconstructed images, as shown in Fig. 3.

2.3 Filtered Back-Projection

The obvious way to reconstruct original image im is the following:

$$im(x,y) = F^{-1} \frac{M(u,v)}{H(u,v)} \tag{7}$$

where F denotes the Fourier transform. But, retrieving im as shown in Eq. 7 is unstable as H tends to be zero or very small at multiple frequencies.

(a) PSNR = 18.13   (b) PSNR = 14.42   (c) PSNR = 17.42

(d) PSNR = 18.34   (e) PSNR = 13.84   (f) PSNR = 17.18

(g) PSNR = 17.92   (h) PSNR = 13.62   (i) PSNR = 16.65

Fig. 3. Reconstruction by least squared error estimate with the 52 shortest projection angles and (a, b, c): 10 training images, (d, e, f): 100 training images, (g, h, i): 500 training images

In [15], $H_{p,q}(u,v)$ is regularized with a weighted filter so that the central region has no holes. The image is then reconstructed by direct deconvolution of the filtered PSF with the Mojette back-projected image (Fig. 4). This is equivalent to regularizing the back-projected image in the frequency domain and then taking the inverse Fourier transform. Extremely low values (below a fixed threshold) in the FFT of the filtered PSF are replaced by the mean evaluated over neighborhoods of fixed size. The PSF filtration in [15] is described by:

$$PSF_{modified} = \begin{cases} PSF. \times wnp : K > 1 \\ PSF. \times tnp \ : K < 1 \end{cases}$$

(a) PSNR = 26.32   (b) PSNR = 22.55   (c) PSNR = 23.04
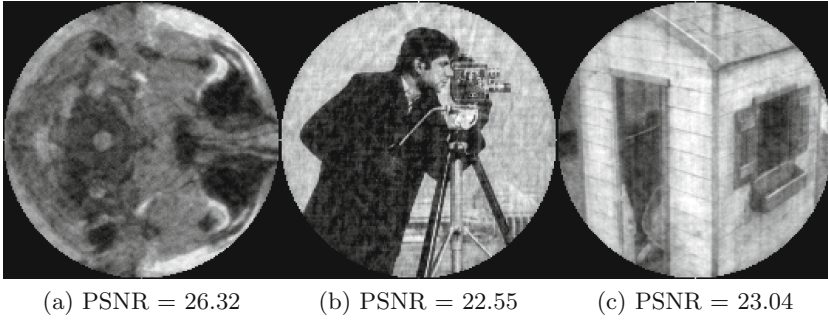
Fig. 4. Reconstruction by the filtered back-projection with the 52 shortest projection angles

(a)   (b)   (c)   (d)
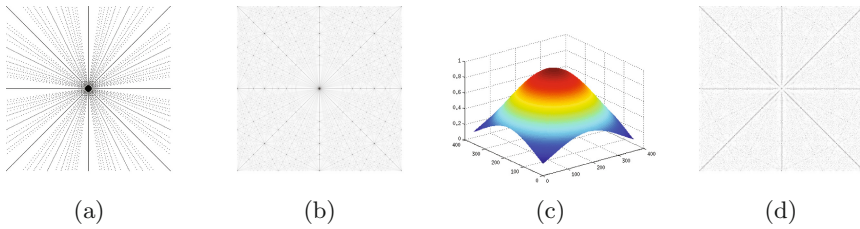
Fig. 5. (a): raw PSF (inverted); (b): FFT of PSF (center-shifted and inverted); (c): The *wnp* filter for a 179×179 image, measured using the 52 shortest Mojette angles; (d): absolute difference between FFT of raw PSF and filtered PSF (center-shifted and inverted)

where $.\times$ denotes 'point-to-point' multiplication and $K = k/N$; k being the Katz number given by: $k = 1 + max(\sum_i |p_i|, \sum_i |q_i|)$ [9] and $N \times N$ being the dimension of the image. The Katz number is dependent not only on the number of views but also on the specific set of angles (p, q) chosen. The filter *wnp* is computed [15] by cross-correlating the back-projected images *wp* and *wn*; *wp* being generated by back-projecting delta image along the set of angles that was used while taking measurements and *wn* being generated by back-projecting delta image along complementary set of angles.

$$wnp = (wp \star wn) \star (D \star D) \tag{8}$$

$$tnp = (wp \star wn) \tag{9}$$

where D is 1 within the region of interest and $\star$ denotes cross-correlation. The *wnp* filter for an image of size 179×179 and measurements taken along the 52 shortest angles, is shown in Fig. 5. A big advantage of this approach is that it can accommodate, with small drop in performance, angle distributions that are uniform, random or clumped.
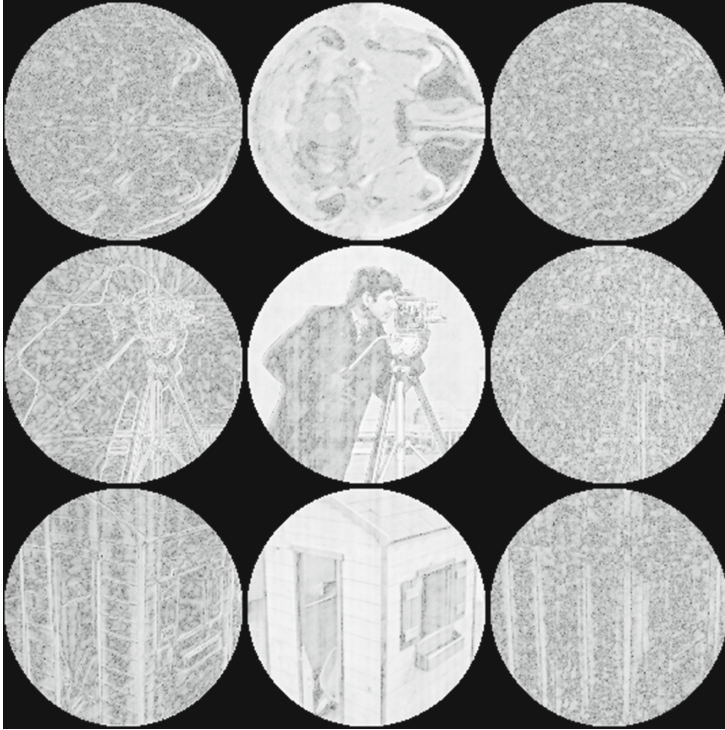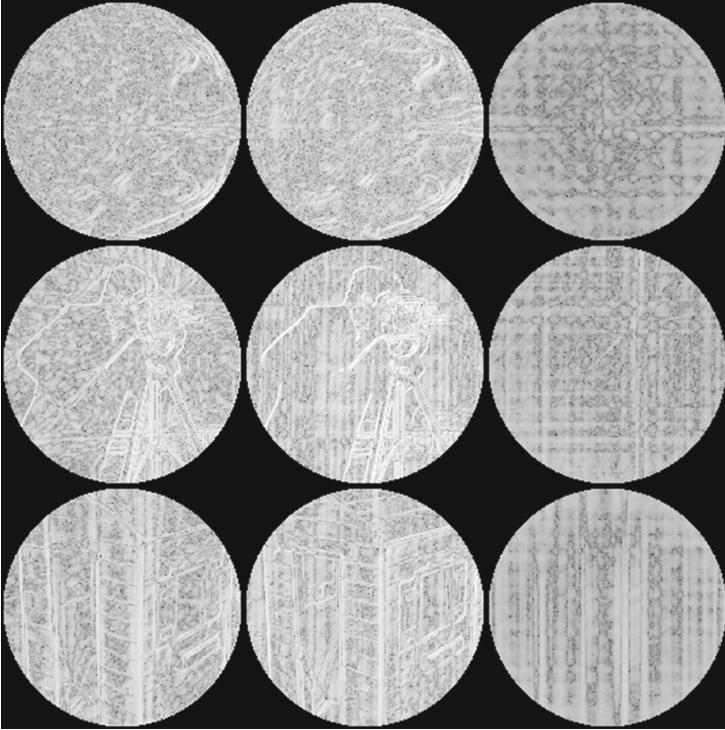
Fig. 6. Absolute error (in log scale to accentuate small intensity differences) on applying different direct reconstruction techniques using the shortest 52 projection angles. Left column: Radon-iRadon; Middle column: least squared error reconstruction; Right column: filtered back-projection reconstruction for images of brain (top row), cameraman (middle row) and house (bottom row)

2.4   Comparison of Different Reconstruction Techniques

The absolute errors in reconstruction by all the above techniques are shown in Figs. 6 and 7 in logarithmic scale, while the reconstructions on rotated images are shown in Fig. 8. The errors in Radon-iRadon and more so, in least squared error based methods are strongly dependent on image structure. However, in the filtered back-projection, for a sufficient number of projection views, a significant portion of the error is image independent, indicating scope for improvement in this technique.

For example, when the number of projection views was 52, errors of all methods were dependent on image structure, as shown in Fig. 6. But, when the number of views was increased to 200, the errors in the filtered back-projection method alone was weakly dependent on the image structure (Fig. 7), whereas the errors in other two methods still showed strong image dependency.

The PSF model is simple and makes no assumptions about the back-projected data. The image reconstruction is very fast and avoids any concern

Fig. 7. Absolute error (in log scale to accentuate small intensity differences) on applying different direct reconstruction techniques using the shortest 200 projection angles. Left column: Radon-iRadon; Middle column: least squared error reconstruction; Right column: filtered back-projection reconstruction for images of brain (top row), cameraman (middle row) and house (bottom row)

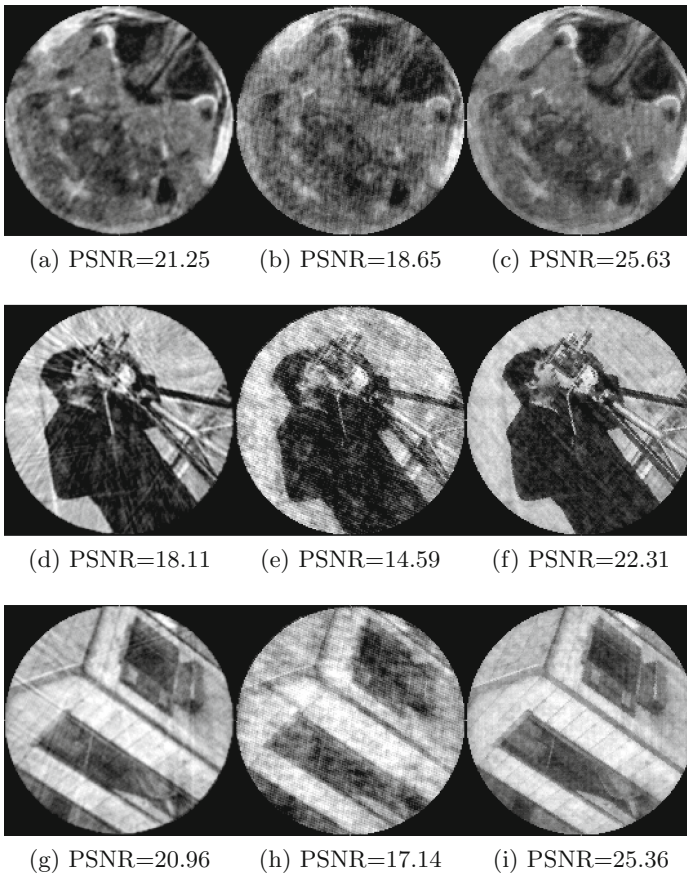over convergence rates and local minima in optimization that may constrain iterative methods.

3   Improved Filtered Back-Projection for Mojette Inversion

We wish to investigate ways to improve the filtered back-projection method, because it gives better results than the other two techniques. First, we discuss the sensitivity of this method to the value of threshold and then the strong effects of selecting particular angles as part of the projection set.

3.1   Replacing Holes in the Fourier Domain of the Filtered Point Spread Function

In filtered back-projection, the FFT of the filtered PSF is checked for values lower than a threshold. Such values are replaced by mean of their neighborhood [15].

(a) PSNR=21.25   (b) PSNR=18.65   (c) PSNR=25.63

(d) PSNR=18.11   (e) PSNR=14.59   (f) PSNR=22.31

(g) PSNR=20.96   (h) PSNR=17.14   (i) PSNR=25.36

Fig. 8. Reconstruction on rotated images of brain (top row), cameraman (middle row) and house (bottom row) using Radon-iRadon (left column), least squared error method (middle column) and filtered back-projection (right column) with the 52 shortest projection angles
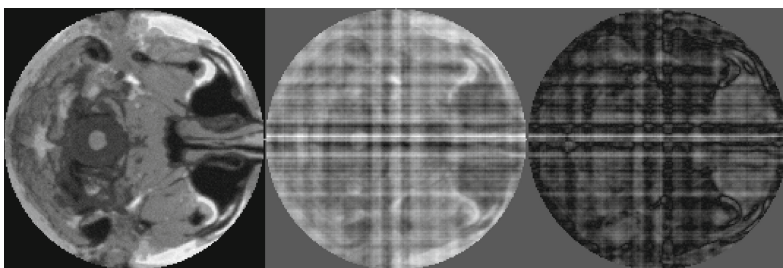
Fig. 9. Reconstruction with the shortest 50 angles excluding the angles: (0,1) and (1,0); Left: original Image; Middle: reconstructed image; Right: absolute error

Table 1. Variation of optimal threshold (fval) with image size and Katz ratio. The optimal threshold is the smallest threshold corresponding to the PSNR that lies within 0.01 of the global maximum PSNR, computed for resized versions of the cameraman image

Katz ratio	Image size: 179×179			Image size: 89×89			Image size: 43×43		
	# shortest angles	Peak PSNR	fval	# shortest angles	Peak Peak	fval	# shortest angles	Peak PSNR	fval
0.46	33	16.6	13	21	18.13	8	13	17.65	8
0.7	44	20.52	16	28	21.36	10	17	20.12	7
0.88	52	22.39	15	32	22.26	11	20	22.2	8
1.10	60	23.58	14	38	23.63	11	24	23.36	7
1.30	64	24.24	15	42	24.69	11	25	24.34	8
1.75	81	26.51	13	50	26.75	10	31	26.44	9
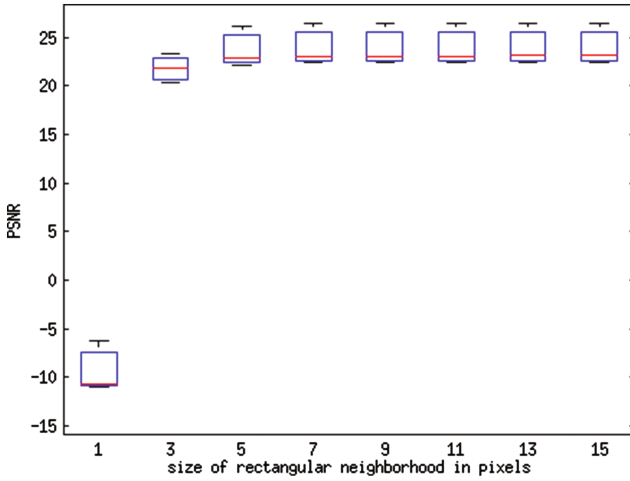
Fig. 10. Observing the quality of reconstruction as the size of neighborhood over which mean is evaluated is varied in each of the three images. The middle red line represents median and the ends of the boxes represent the 25th and 75th percentiles of PSNRs (Color figure online).

We observed the quality of reconstruction for different values of threshold. The optimal threshold is slightly dependent on image size, as seen in Table 1. This is because a larger sized PSF has higher frequency content (requiring a relatively higher threshold). However, the sensitivity of image reconstructions to the selected value of the threshold is quite weak over a wide range of image sizes and Katz values. We also observed (Fig. 10) how the size of neighborhood over which the mean is evaluated, affects the quality of reconstruction. Based on this information, we have used a 5×5 neighborhood.

3.2   Choice of Discrete Angles

Guillaume de Charette [16] and Matúš *et al.* [12] studied the amount of variance captured by different discrete angles. They observed that a discrete angle (p, q) captures variance (or information) proportional to $\frac{1}{p^2+q^2}$. Our observation confirms this. Figure 9 shows reconstructed image when angles $(0, 1)$ and $(1, 0)$ were omitted. The resultant reconstructed image has strong errors along $0°$ and $90°$. Hence, even when random set of angles is used, it is essential to include shorter angles like $(1, 0)$, $(0, 1)$, $(1, 1)$ and $(-1, 1)$. This effect might be compensated for by improved design of the weighting filter wnp.

4   Conclusion

We have compared three related techniques for direct image reconstruction from a finite set of discrete projections. We observed that as the number of projections increases, the reconstruction errors in filtered back-projection method is least dependent on the image structure and orientation. Hence, there is good scope for further improvement in this method. Ideally, we would like to modify the filter such that there is no need for a final threshold based clipping. Towards this, we observed how this optimal threshold depends on image size and Katz number.

References

1. Smith, K., Solmon, D., Wagner, S.: Practical and mathematical aspects of the problem of reconstructing objects from radiographs. Bull. Am. Math. Soc. **83**(6), 1227–1270 (1977)
2. Recur, B., Desbarats, P., Domenger, J.-P.: Radon and Mojette projections' equivalence for tomographic reconstruction using linear systems. In: 16-th International Conference in Central Europe on Computer Graphics, Visualization and Computer Vision 2008, Plzen, Czech Republic (2008). https://hal.archives-ouvertes.fr/hal-00353145
3. Guédon, J., Barba, D., Burger, N.D., Wagner, S.: Psychovisual image coding via an exact discrete radon transform. Bull. Am. Math. Soc. **2501**, 562–572 (1995)
4. Servieres, M.C.J., Normand, N., Subirats, P., Guédon, J.: Some links between continuous and discrete radon transform. In: Fitzpatrick, J.M., Sonka, M. (eds.) Medical Imaging 2004: Image Processing. Society of Photo-Optical Instrumentation Engineers (SPIE) Conference Series 1961–1971, vol. 5370, May 2004
5. Serviéres, M., Normand, N., Guédon, J.P.: Interpolation method for Mojette transform. In: SPIE-Medical Imaging: Image Processing, vol. 6142 (2006)
6. Svalbe, I., Kingston, A., Guédon, J., Normand, N., Chandra, S.: Direct inversion of mojette projections. In: 20th IEEE International Conference on Image Processing (ICIP), September 2013, pp. 1036–1040 (2013)
7. Guédon, J.: The Mojette Transform: Theory and Applications. ISTE, London; Wiley, New Jersey (2009)
8. Guédon, J.-P., Normand, N.: The Mojette transform: the first ten years. In: Andrès, É., Damiand, G., Lienhardt, P. (eds.) DGCI 2005. LNCS, vol. 3429, pp. 79–91. Springer, Heidelberg (2005)

9. Katz, M.: Questions of Uniqueness and Resolution in Reconstruction from Projections. Lecture Notes in Biomathematics, vol. 26. Springer, Heidelberg (1978)
10. Logan, B.F.: The uncertainty principle in reconstructing functions from projections. Duke Math. J. **42**(4), 661–706 (1975)
11. Gopal, P., Chandran, S., Svalbe, I., Rajwade, A.: Multi-slice tomographic reconstruction: to couple or not to couple. In: IEEE International Conference on Image Processing (ICIP) (2016, Submitted)
12. Matúš, F., Flusser, J.: Image representation via a finite radon transform. IEEE Trans. Pattern Anal. Mach. Intell. **15**(10), 996–1006 (1993)
13. Kingston, A., Li, H., Normand, N., Svalbe, I.: Fourier inversion of the Mojette transform. In: Barcucci, E., Frosini, A., Rinaldi, S. (eds.) DGCI 2014. LNCS, vol. 8668, pp. 275–284. Springer, Heidelberg (2014)
14. Cocosco, C.A., Kollokian, V., Kwan, R.K.S., Pike, G.B., Evans, A.C.: BrainWeb: online interface to a 3D MRI simulated brain database. NeuroImage **5**, 425 (1997)
15. Svalbe, I., Kingston, A., Normand, N., Der Sarkissian, H.: Back-projection filtration inversion of discrete projections. In: Barcucci, E., Frosini, A., Rinaldi, S. (eds.) DGCI 2014. LNCS, vol. 8668, pp. 238–249. Springer, Heidelberg (2014)
16. de Charette, G.: Data encryption using the finite radon transform. École Polytechnique de l'Université de Nantes, Monash University, Technical report, Département Informatique (2010)